A novel Zn–TiO$_2$/C@SiO$_2$ nanoporous material on rice husk for photocatalytic applications under visible light

Hui Chen[a], Lei Zhao[a], Ying Xiang[b], Yu He[b], Gongwu Song[b,*], Xitang Wang[a], Feng Liang[a]

[a]*The State Key Laboratory of Refractories and Metallurgy, Wuhan University of Science & Technology, Wuhan 430081, P.R. China,*
Tel. +86 27 68862833; Fax: +86 27 6886833; emails: 280507805@qq.com (H. Chen), wustzhao@163.com (L. Zhao),
461681189@qq.com (X. Wang), 258333753@qq.com (F. Liang)
[b]*Hubei Collaborative Innovation Center for Advanced Organic Chemical Materials, Wuhan 430062, P.R. China,*
Tel. +86 27 50865313; Fax: +86 27 88663043; emails: heyu@hubu.edu.cn (Y. He), songgw@hubu.edu.cn (G. Song)

ABSTRACT

A series of self-nitrogen-doped and Zn-doped TiO$_2$/C@SiO$_2$ (ZTRH) nanoporous composites with high surface area and excellent biological hierarchical porous structure have been synthesized by sol–gel method at different temperatures. The porous SiO$_2$ and activated carbon from the decomposition of rice husk (RH) were regarded as the template and porous catalytic carrier. The structure, crystallinity, morphology, and other physical–chemical properties of the samples were characterized by X-ray diffraction, transmission electron microscopy, X-ray photoelectron spectroscopy, Fourier transforminfrared spectroscopy, N$_2$ adsorption–desorption isotherms, and UV–vis diffuse reflectance spectroscopy. The feasibility of ZTRH nanoporous composites for decomposing pollutants was evaluated by rhodamine B under visible light irradiation. Compared with the traditional photocatalytic materials, ZTRH nanoporous materials not only performed high efficiency in pollutants degradation, but also exhibited good adsorption properties. Moreover, since RH ash acts as the catalyst support, the composites are easily recycled after catalysis reaction. The ZTRH nanoporous composites could be applied to the wastewater with different pH values and be regarded as a kind of promising recyclable photocatalyst in photodegradation of pollutants in water.

Keywords: Zn-doped TiO$_2$/C@SiO$_2$; Rice husk; Photocatalyst; Visible light

1. Introduction

Aromatic pollutants widely present in the effluents containing dyestuffs, pesticides, petrochemicals, and other industries products [1–3] which could be easily loaded to environment and cause health problems to human beings. Photoinduced redox chemical reaction occurring on irradiated semiconductor surface is a kind of promising remediation methodology to surmount this pollution problem, especially for aromatic pollutants [4–7]. Because of its relative high efficiency, non-toxicity, low cost, chemical inertness, and photostability, nanostructured TiO$_2$ has received a considerable attention in aromatic pollutants degradation [5,6]. Despite that great progresses in improving the

*Corresponding author.

photocatalytic performance of nanostructured TiO$_2$ has been achieved in the past decades, there are still some challenges to be addressed, for example, narrow excitation wavelength, fast recombination rate of photogenerated electron–hole pairs, small specific surface area, and difficult recycled after the wastewater treatment [8–11].

To solve those aforementioned problems, nanostructured TiO$_2$ in anatase phase hybrid with hierarchical nanoporous materials with high specific surface areas are desirable since such a hierarchical nanoporous structure offers an alternative strategy to minimize diffusion barriers and potentially provides more active sites for catalyst reactions [12,13]. Meanwhile, immobilizing nanostructured materials on substrate could make the catalysts easily separated and recycled after wastewater treatment [14–16]. However, presynthetic of hierarchical porous substrate to produce the titania replica requires additional processes that might be costly and of environmental concern. The rice husk (RH), consisting of organic components (e.g. cellulose, hemicellulose, and lignin) (61–77 wt.%), ash (mainly amorphous SiO$_2$) (13–29 wt.%) and water, can provide nanoporous SiO$_2$ and activated carbon as excellent catalytic substrates with large specific surface area [17–19]. For instance, biogenic hierarchical TiO$_2$/SiO$_2$ derived from RH with enhanced photocatalytic properties for dye degradation has been studied [20–27]. Titania and ceria incorporated RHs silica has been synthesized for heterogeneous catalyst with high adsorption capability to photodegrade MB under UV irradiation [23,24] or using RH as catalyst support for TiO$_2$ to remove rhodamine B from wastewater [25]. MCM-41 and ZSM-5 zeolites also have been synthesized from RH ash for catalytic reaction [26,27].

So far, since RHs was considered as catalyst carriers because nanostructured SiO$_2$ could be formed inside, it contains substantial concentration of organic substances which can be as a precursor for active carbon-based materials and provide a natural template to obtain nanostructures that requires attentions as well. As we know, Zn^{2+} is a good activating agent to produce activated carbon [19,28] to obtain RH-based porous materials with extra specific surface area 500–1,200 m^2/g which is much higher than 500 m^2/g that achieved by physical method (CO$_2$ gas) [29]. Moreover, the doped Zn^{2+} into TiO$_2$ could significantly alleviate the decay of the light-to-electric energy conversion efficiency at low illumination intensity and extend the excitation wavelength. Indeed, since the band gap of pure TiO$_2$ (anatase) is 3.2 eV, only UV light with a wavelength shorter than 380 nm could be responsive for photocatalysis and it is a crucial limitation for the utilization under visible light [30–33]. The

dopant Zn^{2+} could improve the photocatalytic ability of TiO$_2$ under visible light [34]. Besides, as RH contains abundant non-metallic elements such as N, it indicates that nitrogen in RH could be self-doped into mixed-oxide system during synthesis. Meanwhile, the biological nanoporous structure is hierarchical which plays a fundamental role in photosynthesis and underpins the survival of virtually all higher life forms [20–22].

Herein, we demonstrate a facile method to prepare uniform Zn-doped TiO$_2$/C@SiO$_2$ (ZTRH) nanoporous composites by sol–gel method with RH as a template (Fig. 1). The porous SiO$_2$ and activated carbon from RH function as the template and porous catalytic carrier. The activated carbons not only have high adsorption capacity, but also assist to form *in situ* amorphous carbon layer for fast transfer of hot charge carriers [35,36]. Furthermore, the self-doped N element into mixed-oxide system and Zn–TiO$_2$ located on the surface of porous SiO$_2$ and carbon display excellent catalytic degradation ability of rhodamine B (RhB) under visible light. Compared with the conventional photocatalytic materials, ZTRH nanoporous materials not only exhibit high efficiency in photocatalysis, but also own good properties in pollutant adsorption. Moreover, RHs as the catalyst supporters result in the nanocomposites easy-recycled after catalytic reactions.

2. Experimental

2.1. Materials

All chemicals were analytical grade and used without further purification. Hydrochloric acid (HCl), titanium tetrabutoxide, nitric acid, EtOH, ZnCl$_2$ were purchased from the Sinopharm Group Co. LTD. Distilled water was applied for all the synthesis and treatment processes. The RH was from Jingmen of Hubei Province in China.

2.2. The synthesis of ZTRH nanoporous materials

ZTRH nanoporous composites were synthesized in a step wise method via sol–gel reaction. Forty grams of clean RHs were stirred in 600 ml HCl (1 wt.%) at 100°C for 1 h. Acid-treated RHs were washed with distilled water to pH 7.0 and dried in an oven at 100°C for 24 h to obtain the product (Acid treated RH, HRH). About 10 g HRH was added to 50 ml 10 wt.% ZnCl$_2$, then stirred for 1 h at room temperature, and dried in an oven at 100°C for 24 h to obtain Zn-RH (ZRH). The titania sols were prepared according to literature [37]. Ten gram-pretreated ZRH was added into 50 ml titania sols and impregnated for 24 h, after
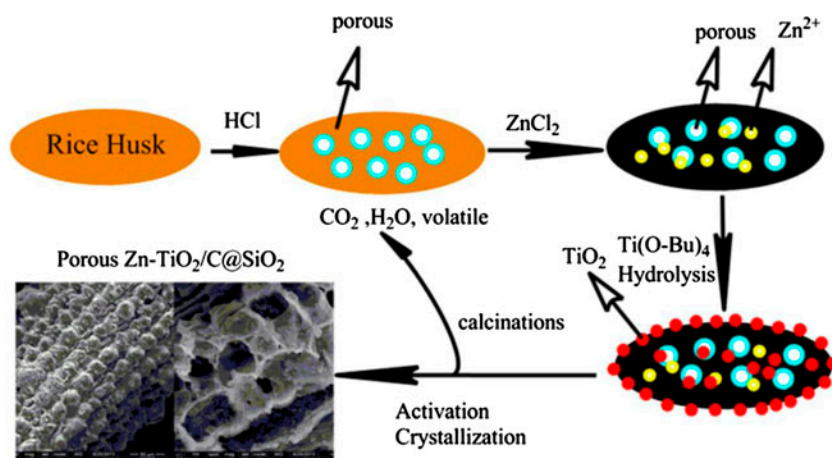
Fig. 1. The proposed formation mechanism of ZTRH nanoporous composites.

which the mixtures were dried in an oven at 100°C for 24 h to obtain the precursor of ZTRH nanoporous composites. For facilitating the performance of the sample, the RH without $ZnCl_2$ treating was also added into titania sols and impregnated for 24 h to obtain the precursor of $TiO_2/C@SiO_2$ nanoporous composite (TRH). The precursor of ZTRH and TRH was heat treated at different temperatures (450, 550, and 650 C) for 3 h with a heating speed of 3 C/min in a flow of nitrogen (1.0 L/min) in a tubular electric furnace to obtain the products. The synthesized ZTRH and TRH were coded as ZTRH450, ZTRH550, ZTRH650, TRH450, TRH550, and TRH650, respectively, according to the various heated temperature.

2.3. Characterizations

In order to determine the crystalline phases of the heat-treated powder samples, X-ray diffraction (XRD) measurements (XRD, X'Pert Pro, Philips, Netherlands) were carried out using a conventional Bragg–Brentano diffractometer with Ni-filtered Cu Kα radiation. The morphology of the samples was examined by a field emission scanning electron microscope (FESEM, Quanta 400, FEI Company, USA) equipped with an energy dispersive X-ray spectroscope (EDS, Noran 623M-3SUT, Thermo Electron Corporation, Japan) and transmission electron microscopy (Transmission electron micros-copy (TEM), JEM-2100UHRJEOL, Japan). The Brunauer–Emmett–Teller (BET) surface areas and porosities of the samples were studied with a nitrogen adsorption instrument (Micrometrics ASAP 2020). Fourier transform infrared (FTIR) spectra were taken with a spectrum one FTIR spectrophotometer (Perkin-Elmer, America) at room temperature. The absorption spectra were carried on by Lambda 35 spectrophotometer (Perkin-Elmer, America). Photocatalytic oxidation of the organic compounds occurred under the illumination of a 500 W xenon lamp equipped with a 420 nm cut-off filter. UV–vis absorption spectroscopy of all of the samples was recorded using a Varian Cary UV–vis–NIR spectrophotometer in the spectral range 200–800 nm. 0.25 g of each sample was pressed between two pieces of quartz glass within the 363 cm area to cover the aperture through which the excitation light passed. A $BaSiO_4$ plate was used as the basic line for the spectra. The element composition and chemical oxidation state were investigated by X-ray photoelectron spectra (XPS) on a VG Multi lab 2000 spectrometer (Thermo Electron Corporation) with Al Kα radiation as the exciting source (300 W). Binding energies were calibrated versus the carbon signal at 284.64 eV.

2.4. Photocatalytic reactions

The photocatalytic activity of ZTRHs was demonstrated by a photocatalytic degradation of RhB with concentration at 40 μM in water. In a 25 mL of RhB aqueous solution, 0.025 g catalyst was suspended and the solution was stirred in a dark room for 1 h to reach the absorption equilibrium. The solution was irradiated by a 500 W xenon lamp with a 420 nm cut-off filter in an open thermostatic photo reactor. At a given time interval of irradiation, the concentration of RhB in the solution was analyzed using a Lambda 35 spectrophotometer. The degradation rate of the RhB was evaluated by the equation:

$$(D) = \frac{[A_0 - A]}{A_0} \times 100\% = \frac{[C_0 - C]}{C_0} \times 100\% \qquad (1)$$

where A and A_0 are the absorbance of RhB solution after and before degradation, C and C_0 are the concentration of RhB after and before degradation.

3. Results and discussion

3.1. Characterizations of samples

3.1.1. Morphology

Fig. 2 showed the SEM images of RH (Fig. 1(a) and (c)) and ZTRH550 (Fig. 2(b) and (d)). The outer surface of lemma was high ridge with a linear profile (Fig. 2(a)). Underlying the outer epidermis were two layers of thick-walled fibers (Fig. 2(c)). The two layers made up sandwich structure-like honeycomb with homogeneous superfine porosities, resulted in

excellent absorb properties of RH. In Fig. 2(b) and (d), ZTRH550 was coated by the TiO$_2$ nanoparticles. These biomorphic high ridges can turn into active sites for catalytic degradation. Moreover, the internal tissue of ZTRH550 displayed hierarchical biological porous structure. The pore with the diameter of 10–15 μm along the entire length of ZTRH550 can provide high adsorption capacity and specific surface area. The SEM images and the corresponding EDS spectrum (Fig. 2(a) and (c)) confirmed the presence of C, Si, and O elements in the heat-treated RH, while the TiO$_2$ particles formed a thin film coating on the RH surface of ZTRH550 can be confirmed by the SEM-EDX technique (Fig. 2(b) and (d)).

The TEM images of ZTRH550 are displayed in Fig. 3. Fig. 3(a) exhibits the agglomeration of TiO$_2$
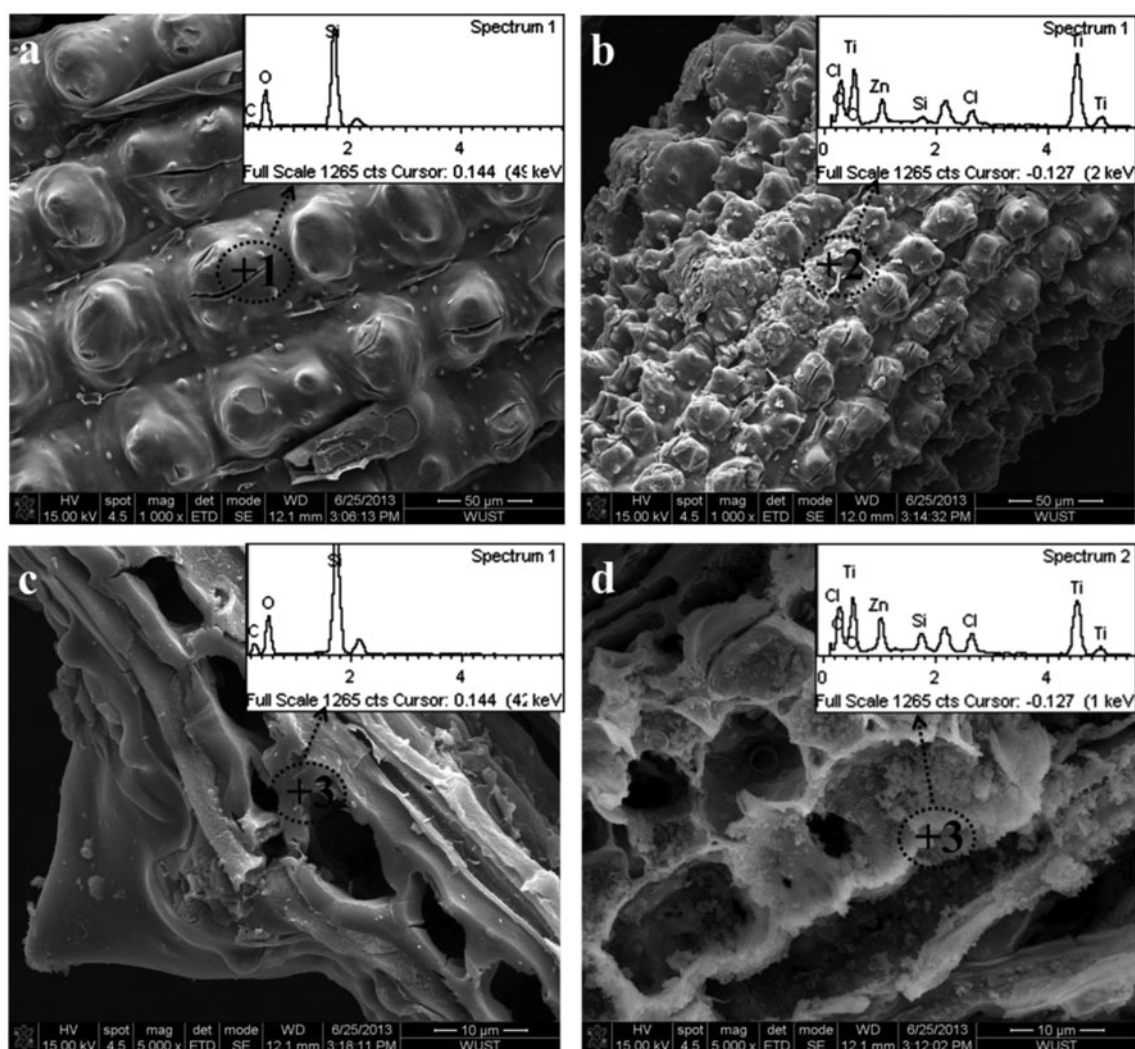

Fig. 2. SEM images of RH (a,c) and ZTRH550 (b,d). The EDS spectrum of RH and ZTHR 550 were inset in corresponding spectrum.
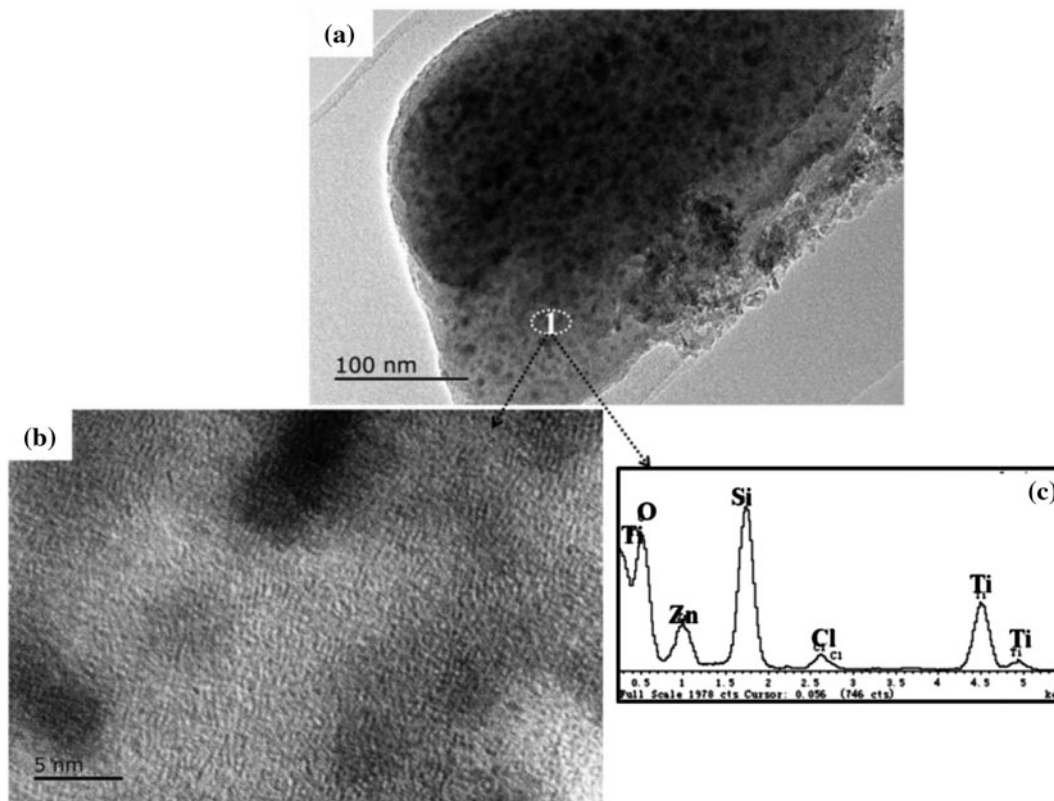
Fig. 3. TEM images (a) and HRTEM image (b) of ZTRH550, EDX spectrum of point 1 (c).

supported on porous RH SiO$_2$. It shows a worm-hole-type porosity of uniform nanopores. In this view, most of TiO$_2$ particles were well distributed across the nanoporous ZTRH550 (Fig. 3(a) and (b)), which confirmed the regularity of the internal structure of catalysts and registered a good aspect of prepared catalysts for photocatalytic degradation of RhB. EDX spectra in Fig. 3(c) demonstrates that it contains O, Si, Ti, Cl, and Zn elements at point 1 within the ZTRH550 particles as shown in Fig. 3(a).

3.1.2. Surface area and pore size distribution

The nitrogen adsorption–desorption isotherms of ZTRH550 are shown in Fig. 4. The form of N$_2$ adsorption–desorption isotherm curves indicated that ZTRH550 was mesoporous materials. In Fig. 4, the pore sizes on the nanoscale for the ZTRH550 were distributed between 1 and 40 nm, centered around 2 nm. The specific area of the TRH calcined at 550 C (TRH550) and ZTRHs calcined at 450, 550, and 650°C were 145.9, 219.2, 319.2, and 343.5 m^2 g^{-1}, respectively (In Table 1). The specific area of the ZTRH samples increased with the calcination temperature increased

from 450 to 650°C. The specific area of ZTRHs calcined at 450, 550, and 650°C was larger than the TRH550 demonstrated the addition of Zn could obviously increase the specific area of the ZTRH samples.
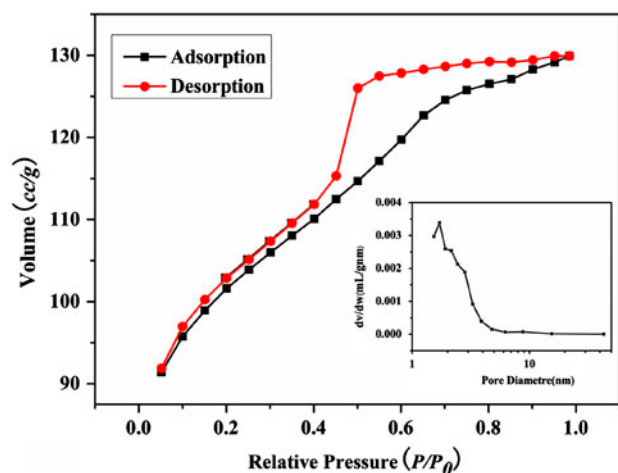

Fig. 4. The nitrogen adsorption–desorption isotherm and pore size distribution of ZTRH550.

Table 1
BET surface area of TRH and ZTRHs calcined at different temperature

Samples	BET surface area/m^2 g^{-1}
TRH550	145.9
ZTRH450	219.2
ZTRH550	319.2
ZTRH650	343.5

3.1.3. FTIR spectral analysis

Fig. 5(a) described the FTIR spectra of RH, TRH550, and ZTRH550. And, Fig. 5(b) shows the FTIR spectra of ZTRH450, ZTRH550, and ZTRH650. The broad band near 3557 and 1614 cm^{-1} appeared in all the FTIR curves were, respectively, ascribed to the stretching and bending modes of the surface hydroxyl groups (including SiO$_2$–OH, C–OH, and TiO$_2$–OH). It demonstrated that the presence of silicon and carbon could increase the contents of both chemisorption and physisorption hydroxyl groups on the surfaces of the nanoporous composites [38]. The hydroxyl was important in the TiO$_2$ catalyst because it not only reduced the recombination of electron-hole pairs but also had a strong photo-oxidation capability that can improve the photocatalystic activity of the TiO$_2$ catalyst. The band at 880–993 cm^{-1} can be observe in a-(B), a-(C), b-(a), b-(b), b-(c), but not in a-(A) was attributed to asymmetric Si–O–Ti stretching vibration of the structural siloxane bond [39], which implied the incorporation of titanium into the framework of silica.

3.1.4. UV/VIS spectra

Fig. 6 shows the UV–vis absorbance spectra of TRH550, ZTRH450, TRH550, and TRH550, respectively. ZTRH exhibited huge absorption spectra in UV–vis range and presented black color. The absorption in the visible-light region implies that the prepared samples can be activated by visible light to form photogene-rated electrons and holes and participate in the desired photocatalytic reactions. As confirmed by XPS analysis (Fig. 7), additional amount of N and Zn was doped into the TiO$_2$. TRH550, however, exhibited relatively lesser absorbance as compared to ZTRH, due to the surface deposition of Zn–TiO$_2$.

3.1.5. X-ray photoelectron spectroscopy

Fig. 7 shows the XPS survey spectra for the surface of ZTRH550. The deposited film contained Ti, O, Zn, C, and N elements in ZTRH550. The C1s peak is due to the adsorbed carbon. The photoelectron peak for Ti2p can be seen at a binding energy (Eb) of 465 eV, so does O1s at Eb = 537, C1s at Eb = 284.8, and Zn2p at Eb = 1022.2 eV. Si and C contained in the original RH were passed on to ZTRH. The whole XPS survey (Fig. 7(a)) demonstrated that Zn and N exist in the oxides. XPS spectra of Zn 2p region are given in
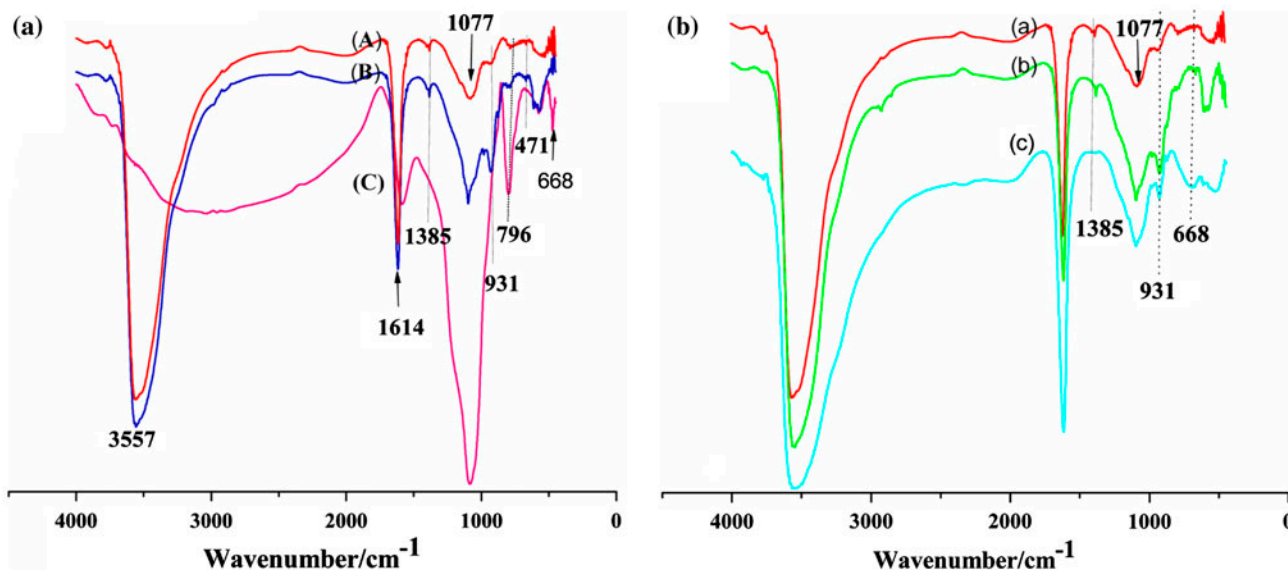

Fig. 5. FTIR spectra of catalysts (a-(a): RH550, a-(B): TRH550, a-(C): ZTRH550, a-(a): ZTRH450, a-(b): ZTRH450, a-(c): ZTRH450).
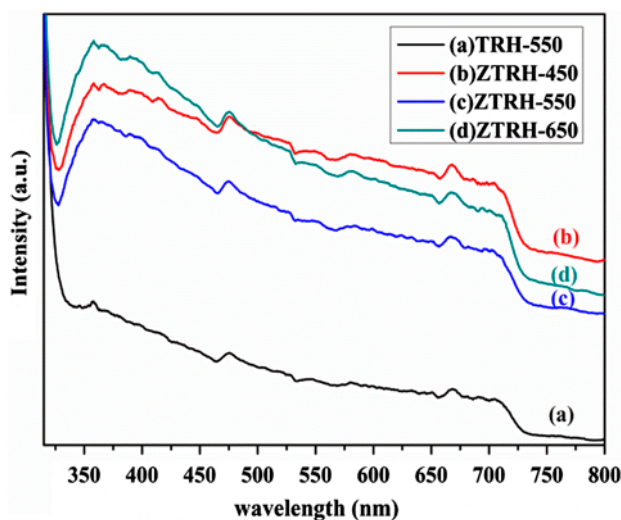
Fig. 6. UV–vis absorbance spectra of TRH550 (a), ZTRH450 (b), TRH550 (c), and TRH550 (d).

Fig. 7(b). Zn (2p3/2, 1/2) doublet was observed at 1022.2 and 1045.1 eV, indicating Zn in 2^+ state bonding with oxygen. The doped zinc has minor influence on titania oxidation state of the ZTRH550 [29,34]. The high-resolution scanning of N 1s displayed in Fig. 7(c) shows three peaks, at 398.2, 400.5, and 401.7 eV, indicating that the N dopants are at the interstitial sites of the TiO_2 lattice [40,41]. The N1S peak at 398 eV is attributed to N anion in O-Ti-N or O-Si-N bonds [42] which is helpful for photocatalytic within the visible range. The latter two peaks are at 400.5 and 401.7 eV, which is assigned to molecularly chemisorbed nitrogen species and helpful for photocatalytic within the visible range [36]. The C1s XPS spectra have four peaks at 284.8, 286.6, 288.7, and 290.5 eV, which are due to C-H bonds, C-O bonds, C=O bonds, and C-N bonds (Fig. 7(d)). These tests demonstrate that Zn and N are co-doped into ZTRH from $ZnCl_2$ and RH.

3.1.6. Powder XRD analysis

XRD analysis was carried out to investigate the changes of TiO_2 phase structure after calcinations as in Fig. 8. Abroad pattern was obtained for RH550, which was typical shape of amorphous solids and suggested the absence of any ordered crystalline structure, indicated relative high disordered structure of silica in this sample. The accompanied rutile phase of TiO_2 was detected in the sample ZTRH450, ZTRH550, and ZTRH650 while anatase phase of TiO_2 was the main crystal phase in ZTRH450 and

ZTRH550. The intensity of peak of TiO_2 anatase phase significantly reduced with increased temperatures but the intensity of rutile phase peak was accordingly increased at the same time. The mean size of a single crystallite can be estimated from full-width at half-maxima of XRD peak by Scherrer's formula:

$$D = \frac{k}{\lambda}\beta\cos\theta \tag{2}$$

The anatase phase crystalline sizes of TiO_2 in ZTRH450, ZTRH550, and ZTRH650 were 5.6, 10.2, and 10.0 nm, respectively. However, the average anatase phase crystalline size of TiO_2 in TRH550 was 3.0 nm. This demonstrated the Zn doping promoted the phase transformation of TiO_2 from anatase phase to rutile phase.

3.2. Photocatalytic activity

Since RhB is a kind of representative pollutant, we use it to evaluate the photocatalytic performance of the TRH and ZTRHs catalyst under visible-light irradiation in this work. In Fig. 9(a), the concentration of RhB decreasing apparently when the irradiation period of visible-light is longer indicated the occurrence of photodegradation of RhB in the system. Nearly 95% RhB was photodegraded in 100 min in the presence of ZTRH450, ZTRH550, and ZTRH650 but no obvious indication about photodegradation of RhB was appeared in the presence of TRH. It indicated that Zn doping played an important role to promote charge transfer between TiO_2 and RhB during the photodegradation of RhB under visible light [30]. Meanwhile, metal oxides with more structure defects on surface could ionosorb oxygen as O^- species and cause hole-trap reaction [14], by which the recombination rate of e^-/h^+ pairs was reduced during the photocatalytic degradation process.

The calculated reaction rate constants of sample ZTRH450, ZTRH550, and ZTRH650 for RhB degradation were 0.0278, 0.0512, and 0.0413 min^{-1}, respectively (Fig. 9(b)). It is noted that the photocatalytic activity of ZTRH500 is higher than others, which is in consistent with the results of XRD. With the increases in calcination temperature from 450 to 550℃, the content of anatase phase and the specific surface area in the ZTRH samples increase. But when temperature is up to 650℃, anatase phase and the specific surface area turn to decrease. The
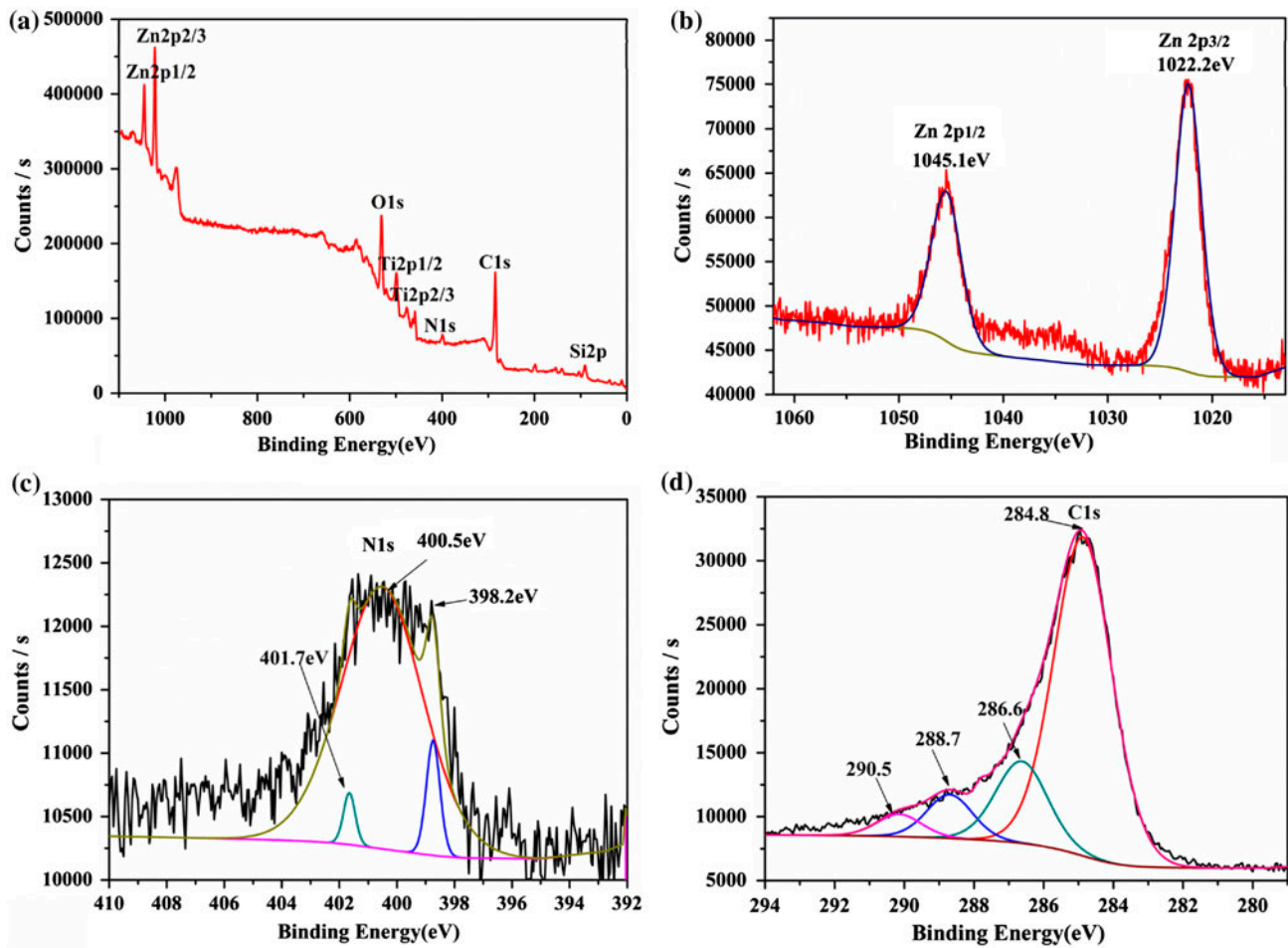
Fig. 7. XPS patterns of ZTRH550. (a) The whole survey; (b) high-resolution spectra of Zn2P; (c) high-resolution spectra of N1S; and (d) high-resolution spectra of C1S.
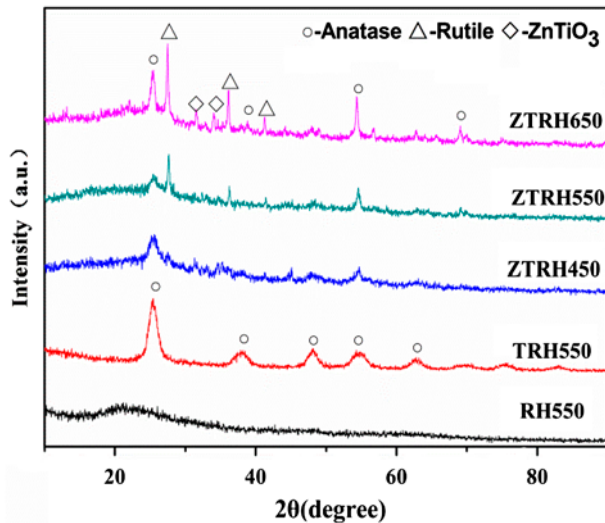

Fig. 8. The XRD patter of RH550, TRH550, and ZTRHs.

enhanced photocatalytic oxidation activity for ZTRHs nanoporous composites under visible light is elucidated in Fig. 10. The active carbon improves the adsorption performance of ZTRHs powder with the graphite structure on the edge to form acidic functional groups for high photocatalytic activity [43]. Moreover, the active carbon enhances the conductivity of TiO_2 to induce rapid transfer of hot carriers to the surface and participate in the photoredox reactions [36]. Furthermore, the doped Zn atoms in TiO_2 can increase the photons number e in the photocatalytic reaction to promote the charge transfer between TiO_2 and RhB [30]. The injected electron reacts with the absorbed O_2 on the surface to yield active oxygen radicals (e.g. O^{2-}, $\cdot OH$) which can degrade or mineralize the dyes in system. Thirdly, the self-doping of N, the advantage is much more prominent under visible light.
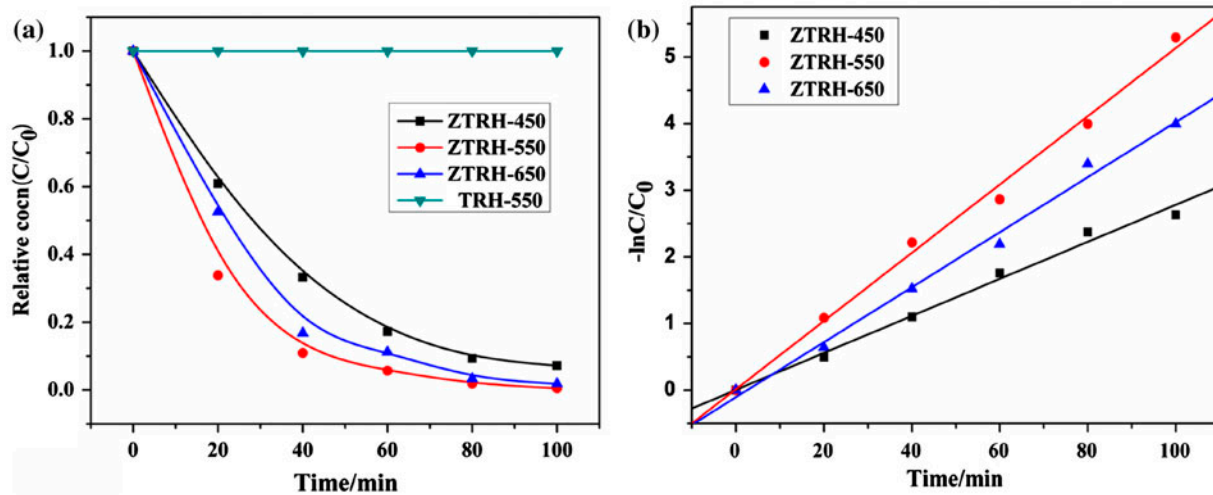
Fig. 9. (a) The kinetic curve of the photodegradation of RhB and (b) Comparison of first-order degradation rates of RhB.
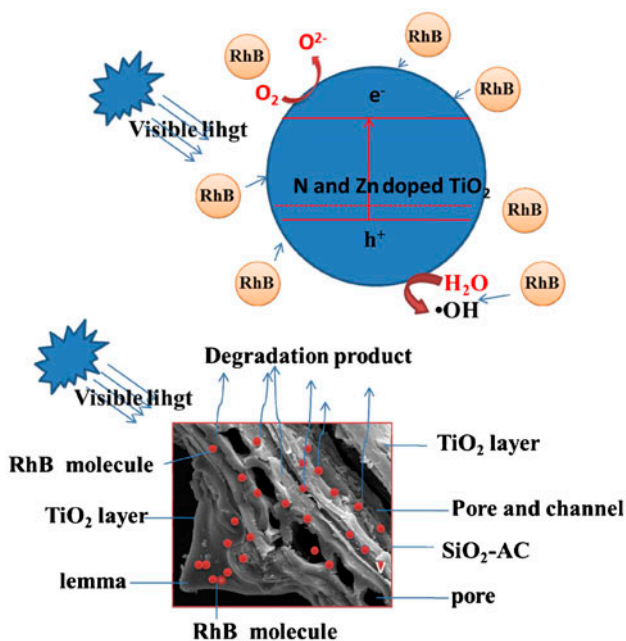

Fig. 10. The schematic illustration of the mechanism of the activation of visible light photocatalytic activity for the ZTRH nanoporous composites.

Fig. 11. Effect of the pH values on photocatalytic degradation of RhB under visible light irradiation.

4. Conclusion

This work employed RH as a biotemplate for the generation of morph-structured TiO_2 by sol–gel method and exhibited the potential application in photodegradation of pollutants in water. The specific area of ZTRHs calcined at 450, 550, and 650°C was larger than the TRH550 demonstrated that the addition of Zn could obviously increase the specific area of the ZTRH samples. This method not only maintained the RH structure but also simultaneously introduced self-nitrogen-doped and Zn-doped in ZTRH sample. The photocatalytic performance of RhB degradation under visible light is better than those prepared with classic routes because of the hierarchical structure feature, the presence of active carbon, and the effective

In Fig. 11, the RhB was photodegraded by ZTRH550 nanocomposites under visible light at different pH values (2.5, 4.0, 6.3, and 10.5). As shown in Fig. 10, the photocatalytic performance of ZTRH550 does not depend on heavily on the pH value. Therefore, the strict chemical environment is not necessary for its application in degradation of wastewater.
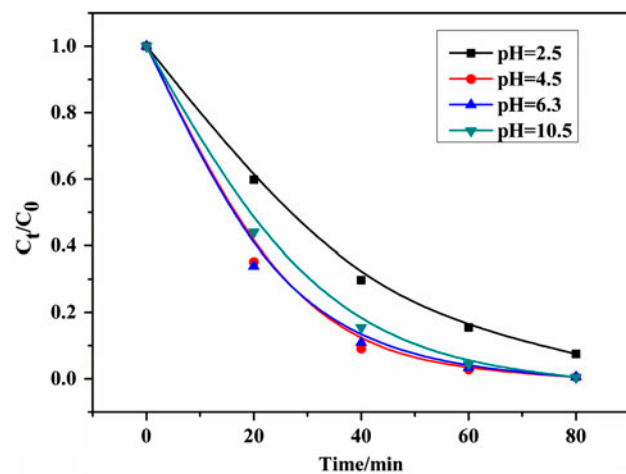
nitrogen and Zn doping during synthesis. Nearly 95% RhB was photodegraded in 100 min in the presence of ZTRH450, ZTRH550, and ZTRH650 but no obvious indication about photodegradation of RhB was appeared in the presence of TRH. Moreover, RH as the catalyst support made the nanocomposites easy-recycled and durability. Owing to above merits, the ZTRH nanoporous materials are a kind of promising recyclable photocatalyst in photodegradation of pollutants in water.

Acknowledgments

References

[1] Y.N. Ho, J.L. Hsieh, C.C. Huang, Construction of a plant-microbe phytoremediation system: Combination of vetiver grass with a functional endophytic bacterium, *Achromobacter xylosoxidans* F3B, for aromatic pollutants removal, Bioresour. Technol. 145 (2013) 43–47.

[2] A. Nzila, Update on the cometabolism of organic pollutants by bacteria. Environmental Pollution, Environ. Pollut. 178 (2013) 474–482.

[3] F. Arena, C. Italiano, G.D. Ferrante, G. Trunfio, L. Spadaro, A mechanistic assessment of the wet air oxidation activity of $MnCeO_x$ catalyst toward toxic and refractory organic pollutants, Appl. Catal. B 144 (2014) 292–299.

[4] L. Biyoghe Bi Ndong, M.P. Ibondou, X. Gu, S. Lu, Z. Qiu, Q. Sui, S.M. Mbadinga, Enhanced photocatalytic activity of TiO_2 nanosheets by doping with Cu for chlorinated solvent pollutants degradation, Ind. Eng. Chem. Res. 53 (2014) 1368–1376.

[5] L.G. Devi, R. Kavitha, A review on non-metal ion doped titania for the photocatalytic degradation of organic pollutants under UV/solar light: Role of photogenerated charge carrier dynamics in enhancing the activity, Appl. Catal. B 140 (2013) 559–587.

[6] J. Schneider, M. Matsuoka, M. Takeuchi, J. Zhang, Y. Horiuchi, M. Anpo, D.W. Bahnemann, Understanding TiO_2 photocatalysis: Mechanisms and materials, Chem. Rev. 114 (2014) 9919–9986.

[7] C. Kim, M. Choi, J. Jang, Nitrogen-doped SiO_2/TiO_2 core/shell nanoparticles as highly efficient visible light photocatalyst, Catal. Commun. 11 (2010) 378–382.

[8] K. Liu, M. Cao, A. Fujishima, L. Jiang, Bio-inspired titanium dioxide materials with special wettability and their applications, Chem. Rev. 114 (2014) 10044–10094.

[9] S. Li, L. Zhang, J. Wang, B. Wang, Y. Li, C. Ma, Preparation of Co-and Cr-doped mixed crystal TiO_2 powders and comparison of the photocatalytic degradation abilities under sunlight irradiation, Desalin. Water Treat. (2014), doi: 10.1080/19443994.2014.908415.

[10] L. Wang, T. Sasaki, Titanium oxide nanosheets: Graphene analogues with versatile functionalities, Chem. Rev. 114 (2014) 9455–9486.

[11] T.K. Le, D. Flahaut, H. Martinez, T. Pigot, H.K.H. Nguyena, T.K.X. Huynh, Surface fluorination of single-phase TiO_2 by thermal shock method for enhanced UV and visible light induced photocatalytic activity, Appl. Catal. B 144 (2014) 1–11.

[12] M.R. Golobostanfard, H. Abdizadeh, Hierarchical sol-gel derived porous titania/carbon nanotube films prepared by controlled phase separation, Microporous Mesoporous Mater. 183 (2014) 74–80.

[13] W. Chen, Z. Ma, X. Pan, Z. Hu, G. Dong, S. Zhou, M. Peng, J. Qiu, Core@dual-shell nanoporous SiO_2-TiO_2 composite fibers with high flexibility and Its photocatalytic activity, J. Am. Ceram. Soc. 97 (2014) 1944–1951.

[14] S. Horikoshi, S. Sakamoto, N. Serpone, Formation and efficacy of TiO_2/AC composites prepared under microwave irradiation in the photoinduced transformation of the 2-propanol VOC pollutant in air, Appl. Catal. 140 (2013) 646–651.

[15] X. Yu, X. Gao, Z. Lu, X. Liu, P. Huo, X. Liu, D. Wu, Y. Yan, Preparation and photodegradation properties of transition metal ion-poly-o-phenylenediamine/TiO_2/ fly-ash cenospheres by ion imprinting technology, RSC Adv. 3 (2013) 14807–14813.

[16] M.G. Alalm, A. Tawfik, S. Ookawara, Solar photocatalytic degradation of phenol by TiO_2/AC prepared by temperature impregnation method, Desalin. Water Treat. (2014), doi: 10.1080/19443994.2014.969319.

[17] V.B. Carmona, R.M. Oliveira, W.T.L. Silva, L.H.C. Mattoso, J.M. Marconcini, Nanosilica from rice husk: Extraction and characterization, Ind. Crops Prod. 43 (2013) 291–296.

[18] D. Kalderis, S. Bethanis, P. Paraskeva, E. Diamadopoulos, Production of activated carbon from bagasse and rice husk by a single-stage chemical activation method at low retention times, Bioresour. Technol. 99 (2008) 6809–6816.

[19] N. Yalcın, V. Sevinc, Studies of the surface area and porosity of activated carbons prepared from rice husks, Carbon 38 (2000) 1943–1945.

[20] D. Yang, T. Fan, H. Zhou, J. Ding, D. Zhang, Biogenic hierarchical TiO_2/SiO_2 derived from rice husk and enhanced photocatalytic properties for dye degradation, PLoS ONE 6 (2011) e24788.

[21] Y. Lu, X.Y. Wei, Z. Wen, H.B. Chen, Y.C. Lu, Z.M. Zong, J.P. Cao, S.C. Qi, S.Z. Wang, L.C. Yu, W. Zhao, X. Fan, Y.P. Zhao, Photocatalytic depolymerization of rice husk over TiO_2 with H_2O_2, Fuel Process. Technol. 117 (2014) 8–16.

[22] D. Yang, B. Du, Y. Yan, H. Li, D. Zhang, T. Fan, Rice-Husk-Templated hierarchical porous TiO_2/SiO_2 for enhanced bacterial removal, ACS Appl. Mater. Interfaces 6 (2014) 2377–2385.

[23] F. Adam, L. Muniandy, R. Thankappan, Ceria and titania incorporated silica based catalyst prepared from rice husk: Adsorption and photocatalytic studies

of methylene blue, J. Colloid Interface Sci. 406 (2013) 209–216.

[24] F. Adam, J.N. Appaturi, Z. Khanam, R. Thankappan, M.A.M. Nawi, Utilization of tin and titanium incorporated rice husk silica nanocomposite as photocatalyst and adsorbent for the removal of methylene blue in aqueous medium, Appl. Surf. Sci. 264 (2013) 718–726.

[25] R. Jain, M. Mathur, S. Sikarwar, A. Mittal, Removal of the hazardous dye rhodamine B through photocatalytic and adsorption treatments, J. Environ. Manage. 85 (2007) 956–964.

[26] S. Artkla, W. Kim, W. Choi, J. Wittayakun, Highly enhanced photocatalytic degradation of tetramethylammonium on the hybrid catalyst of titania and MCM-41 obtained from rice husk silica, Appl. Catal. B 91 (2009) 157–164.

[27] M.M. Mohamed, F.I. Zidan, M. Thabet, Synthesis of ZSM-5 zeolite from rice husk ash: Characterization and implications for photocatalytic degradation catalysts, Microporous Mesoporous Mater. 108 (2008) 193–203.

[28] Y. Chen, Y. Zhu, Z. Wang, Y. Li, L. Wang, L. Ding, X. Gao, Y. Ma, Y. Guo, Application studies of activated carbon derived from rice husks produced by chemical-thermal process—A review, Adv. Colloid Interface 163 (2011) 39–52.

[29] M.J. Prauchner, F. Rodríguez-Reinoso, Chemical versus physical activation of coconut shell: A comparative study, Microporous Mesoporous Mater. 152 (2012) 163–171.

[30] Y. Zhao, C. Li, X. Liu, F. Gu, H.L. Du, L. Shi, Zn-doped TiO_2 nanoparticles with high photocatalytic activity synthesized by hydrogen-oxygen diffusion flame, Appl. Catal. 79 (2008) 208–215.

[31] W. Zhang, S. Zhu, Y. Li, F. Wang, Photocatalytic Zn-doped TiO_2 films prepared by DC reactive magnetron sputtering, Vacuum 82 (2007) 328–335.

[32] Y. Zhang, L. Wang, B. Liu, J. Zhai, H. Fan, D. Wang, Y. Lin, T. Xie, Synthesis of Zn-doped TiO_2 microspheres with enhanced photovoltaic performance and application for dye-sensitized solar cells, Electrochim. Acta 56 (2011) 6517–6523.

[33] K.P. Wang, H. Teng, Zinc-doping in TiO_2 films to enhance electron transport in dye-sensitized solar cells under low-intensity illumination, Phys. Chem. Chem. Phys. 11 (2009) 9489–9496.

[34] R. Hasan, C.W. Lai, S.B.A. Hamid, W.J. Basirun, Z. Lockman, F. Bari, Photoelectrocatalytic activity of Zn-loaded RGO-TiO_2 composite coatings on mild steel substrate via DC electrochemical co-deposition, Eur. Phys. J. Appl. Phys. 65 (2014) 20303.

[35] S. Shanmugam, A. Gabashvili, D.S. Jacob, J.C. Yu, A. Gedanken, Synthesis and characterization of TiO_2@C core-shell composite nanoparticles and evaluation of their photocatalytic activities, Chem. Mater. 18 (2006) 2275–2282.

[36] Y.B. Wang, J.Z. Zhang, X. Liu, S.M. Gao, B.B. Huang, Y. Dai, Y.B. Xu, Synthesis and characterization of activated carbon-coated SiO_2/$TiO_{2-x}C_x$ nanoporous composites with high adsorption capability and visible light photocatalytic activity, Mater. Chem. Phys. 135 (2012) 579–586.

[37] B.A. Morales, O. Novaro, T. Lopez, E. Sanchez, R. Gomez, Effect of hydrolysis catalyst on the Ti deficiency and crystallite size of sol-gel-TiO_2 crystalline phases, J. Mater. Res. 10 (1995) 2788–2796.

[38] F. Mei, C. Liu, L. Zhang, F. Ren, L. Zhou, W.K. Zhao, Y.L. Fang, Microstructural study of binary TiO_2: SiO_2 nanocrystalline thin films, J. Cryst. Growth 292 (2006) 87–91.

[39] X. Zhang, F. Zhang, K.Y. Chan, Synthesis of titania-silica mixed oxide mesoporous materials, characterization and photocatalytic properties, Appl. Catal. A 284 (2005) 193–198.

[40] X. Li, T. Fan, H. Zhou, S.K. Chow, W. Zhang, D. Zhang, Q. Guo, H. Ogawa, Enhanced light-harvesting and photocatalytic properties in morph-TiO_2 from green-leaf biotemplates, Adv. Funct. Mater. 19 (2009) 45–56.

[41] H. Zhou, T. Fan, J. Ding, D. Zhang, Q. Guo, Bacteria-directed construction of hollow TiO_2 micro/nanostructures with enhanced photocatalytic hydrogen evolution activity, Opt. Express 20 (2012) A340–A350.

[42] W. Guo, Y. Shen, G. Boschloo, A. Hagfeldt, T. Ma, Influence of nitrogen dopants on N-doped TiO_2 electrodes and their applications in dye-sensitized solar cells, Electrochim. Acta 56 (2011) 4611–4617.

[43] D. Li, H. Haneda, S. Hishita, N. Ohashi, Visible-light-driven nitrogen-doped TiO_2 photocatalysts: Effect of nitrogen precursors on their photocatalysis for decomposition of gas-phase organic pollutants, Mater. Sci. Eng. B 117 (2005) 67–75.